SIMULTANEOUS AFM-SECM IMAGING OF COPPER DISSOLUTION

J. Izquierdo[1,2,3], B.M. Fernández-Pérez[2], A. Eifert[1], R.M. Souto[2,3], C. Kranz[1]

[1] *Institute of Analytical and Bioanalytical Chemistry, University of Ulm, Albert-Einstein-Allee 11, D-89081 Ulm, Germany.*

[2] *Department of Chemistry, University of La Laguna, P.O. Box 456, E-38200 La Laguna, Tenerife, Canary Islands, Spain.*

[3] *Institute of Material Science and Nanotechnology, University of La Laguna, E-38200 La Laguna (Tenerife), Spain.*

Abstract

Combined atomic force-scanning electrochemical microscopy (AFM-SECM) has been explored for monitoring copper ions generated by dissolution of copper samples while recording induced changes in topography. Released Cu^{2+} ions were detected via reduction to metallic copper at the AFM tip-integrated electrode followed by subsequent re-dissolution in bulk solution by anodic stripping voltammetry. Copper crystals electrodeposited on gold substrates were used as model systems to demonstrate the laterally resolved analysis of topographical changes and the simultaneous measurement of localized cation release, which was anodically activated upon exposure to acidified chloride-containing solution. Finally, the potential of AFM-SECM for monitoring spatially resolved corrosion processes with sub-micrometer resolution was illustrated using a pure copper sample.

Keywords: AFM-SECM; substrate generation-tip collection (SG-TG); electrochemistry; copper corrosion; metal dissolution.

1. Introduction

Metallic corrosion phenomena are related to nanometer- to micrometer-sized defects, although materials may appear homogeneous at the macroscopic level. As a consequence such areas of the surface become activated, forming microgalvanic cells, and hence the onset and the initial stages of the corrosion processes occur within such spatial range. In order to accurately discern the involved mechanisms, the analysis of corrosion processes requires appropriate methods and techniques, which provide laterally resolved information, preferably in real time and under *in situ* corrosion conditions. Typically, scanning vibrating electrode technique (SVET), scanning ion-selective electrode technique (SIET), or localized electrochemical impedance spectroscopy (LEIS) are employed providing spatially resolved chemical and electrochemical information on metallic material undergoing corrosion [1,2]. Also, scanning electrochemical microscopy (SECM) is a highly suitable technique for the investigation of corrosion problems [3,4]. SECM is based on scanning an ultramicroelectrode (UME) in the *x*,*y* plane in close proximity across the substrate surface while locally collecting electrochemical information within the diffusion layer of the solid / liquid interface. The spatial resolution is usually in the sub-micro to micrometer range and is mainly governed by the dimensions of the UME, which typically have radii in the range of 5 to 25 μm.

There are some limitations encountered during conventional SECM operation as the recorded data may have been influenced by more than one parameter. Several factors are contributing to the amperometric response of the UME in any SECM experiment, and in particular during corrosion studies, which can be classified as follows:

(i) Evolution of chemical changes (i.e., composition) of the electrolyte in the vicinity of the substrate surface due to changes of the concentration of involved species. Such changes may be induced by the biased UME and/or related to heterogeneous electron transfer rates at the substrate. This may apply to either species, which are involved in the electrochemical reactions of the corrosion process (i.e., thereby generated or consumed) [5-8], as well as to redox mediators intentionally added for the characterization of the surface [9-13].

(ii) Topographical changes occurring at the sample surface as a result of the corrosion process, which modify the distance between the UME and the sample. Local dissolution and degradation of the sample, along with the precipitation of hydroxides and oxides is expected to facilitate or hinder the diffusion of any electroactive species towards the probe, thus effectively altering the recorded current [14-17].

Nevertheless, SECM is a versatile technique, given that experimental conditions are accurately established, and/or the obtained data are carefully analyzed. SECM provides topographical information, however high resolution topography is more efficiently monitored *in situ* using other scanning probe microscopy (SPM) techniques such as electrochemical atomic force microscopy (EC-AFM), which is of great interest for visualizing corrosion phenomena [18,19]. In EC-AFM, the conductive substrate is part of an electrochemical cell. Nanometer scale changes in surface morphology induced by an electrochemical reaction are monitored with non-conductive silicon or silicon nitride AFM probes. However, spatially resolved electrochemical information, obtainable e.g., by SECM is hardly accessible by EC-AFM.

Over the years, several approaches have been introduced in SECM to minimize the influence of changes in topography on the electrochemical response. Among them, the most promising approaches are the so-called shear-force mode [20,21], the acquisition of frequency-dependent alternating current SECM (AC-SECM) [22-24], and the combination of SECM with

complementary SPM techniques such scanning ion conductance microscopy (SICM) SICM-SECM or atomic force microscopy (AFM) AFM-SECM [25, and references herein]. AFM-SECM is regarded as a particularly attractive tool in corrosion science, as the advantages of both techniques, the unambiguous topographic information provided by AFM and the laterally resolved electrochemical information obtained by SECM, may be obtained in a single experiment. The surface activity and/or changes in the composition of the electrolyte, modified due to the corrosion process, along with the correlative roughness and topography evolution are indispensable in understanding fundamental processes in corrosion. To the best of our knowledge, so far combined AFM-SECM has been applied in corrosion science investigating the heterogeneity in electron transfer of aluminum-based alloyed materials [26-28], or the local induction of corrosion pits on iron [29,30].

Copper is one of the most widely employed metals for industrial applications, which remains passive when exposed to aqueous environments in absence of aggressive conditions such as extreme pH values and/or aggressive species like chloride ions [31-33]. Dynamic degradation-passivation processes occur on copper surfaces when exposed to aggressive media, resulting in the local release of divalent copper cations along with topographical changes. Control of the corrosion process, passivation and cathodic protection of copper materials can be achieved as long as the electric state remains under cathodic potentiostatic control. Changing the potential to more positive values triggers the corrosion, leading to changes in the morphology, which has been monitored *in situ* with EC-AFM [34-36]. Also, SECM has been used to investigate copper corrosion, however, to date the analysis of corroding copper surfaces mostly involves feedback mode investigations using redox mediators for imaging of the surface activity of either inhibited [11,37,38] or intrinsically heterogeneous copper-based substrates [16,39]. Yet, more quantitative data on the dissolution process may be achieved with SECM by amperometrically determining the Cu^{2+} content in solution using under-potential deposition (UPD) in combination with anodic stripping voltammetry at gold UME's [40,41].

Here, we present the potential of AFM-SECM for studying corrosion processes induced by anodically activated surfaces. For proof-of-principle measurements, model samples such as macroscopic planar gold samples (Au-coated silicon wafer or circular gold structures deposited on glass) were electrochemically modified with deposited copper crystals. The release of Cu^{2+} ions from these samples was determined by re-reduction of copper at the AFM tip-integrated electrode, while simultaneously the topographical changes were monitored. In addition, a pure copper substrate was also investigated under potentiostatic control aiming at characterizing phenomena involved with the corrosion process of copper.

2. Experimental

2.1 Reagents and materials

Copper sulphate, potasium chloride and sodium chloride were purchased from Merck (Darmstadt, Germany); sulphuric and hydrochloric acid were obtained from VWR Chemicals (Radnor, PA, USA); and hexaaminruthenium(III) chloride from Sigma-Aldrich (St. Louis, MO, USA). All chemicals were used as received without further purification. All solutions were prepared using analytical grade chemicals dissolved in ultrapure water (Elga water system, conductivity 18.0 MΩ cm; Elga Labwater, VWS Deutschland GmbH, Celle, Germany). All experiments were performed at approximately 20 ºC (room temperature).

As model samples, two different gold substrates were used: a gold-coated silicon wafer (gold layer thickness: 100 nm), and a glass slide with a circular gold coating (50 nm in thickness, diameter 2 mm), which could be electrically connected through a gold line. For the gold-coated silicon wafer, the total exposed gold area was defined by a 1.4 cm diameter o-ring of the electrochemical cell. The deposition of copper at the gold substrates was conducted in 10 mM $CuSO_4$ / 50 mM H_2SO_4 solution. Calibration experiments prior to AFM-SECM imaging were performed in 0.5 M NaCl at pH =3 (the pH was adjusted with hydrochloric acid). This 0.5 M NaCl (pH = 3) solution was also employed during the anodic dissolution of copper at either of the electrodes.

Pure polycrystalline copper samples were prepared from 99.9 % copper sheets (Goodfellow, Cambridge, UK) of 1 mm thickness. According to the manufacturer, the main impurity of this material is silver up to 500 ppm, among other metals below 300 ppm. The sheets were cut into 2.5 cm x 2.5 cm square specimens, ground using silicon carbide papers with increasing grit from 220 to 4000, and subsequently polished with silica colloid micropolish suspension 0.05 µm particle size (Allied High Tech, Rancho Dominguez, CA, USA) until a mirror-like surface was achieved.

All substrates were thoroughly rinsed with ultrapure water, sonicated for 20 minutes in an ultrasonic bath in ethanol for cleaning and degreasing, and finally dried under argon atmosphere. Samples were mounted in the AFM electrochemical cell (Keysight Technologies, Chandler, AZ, USA) and electrically connected as second working electrode. Leakage was prevented with the o-ring, which limits the total exposed area to ca. 1.54 cm^2 for the glass slide with the glass / gold boundary, and 3.14 cm^2 for both the pure copper sample and the gold-coated silicon wafer. The total volumes of the electrochemical cell corresponding to these two exposed areas were 0.5 and 0.7 mL, respectively. A flow-through cell allowed the exchange of the electrolyte solution without changing the AFM tip position in respect to the sample.

2.2 AFM-SECM setup

A 5500 AFM system with SECM module from Keysight Technologies was used for all the imaging experiments reported in this work. The four-electrode setup consisted of a platinum wire counter-electrode, a pseudo-reference electrode (chlorinated silver wire), the AFM-SECM probe as working electrode #1 and the substrate as working electrode #2. The potential of the pseudo-reference electrode was determined with respect to an Ag/AgCl (sat.) reference electrode in all solutions used before and after the experiments, finding no relevant variations. The fabrication of the AFM-SECM probes is described elsewhere [42]. An exemplary SEM image of an AFM-SECM probe used for studying copper dissolution along with its electrochemical characterization in 10 mM $[Ru(NH_3)_6]Cl_3$ / 0.1 M KCl solution is given in **Figure S-2**. The dimensions of the integrated frame electrodes (thickness of the gold layer 100 nm) varied in terms of electrode edge length among the used probes as indicted in the figure captions. In order to obtain curvature radii of the tips similar to commercially available AFM probes, the AFM tip was sharpened by FIB milling and the height of the AFM tip was adjusted in relation to the electrode size (e.g., typical heights were around 400 nm). Electrical connections of the AFM-SECM probes and subsequent re-insulation of the contact point were performed with conductive silver epoxy (PLANO GmbH, Wetzlar, Germany) and UV-sensitive glue (Dymax, Torrington, CT, USA).

All reported potentials are referred to the Ag/AgCl (sat.) reference electrode. Copper cations released from the potentiostatically controlled sample surfaces were electrochemically reduced to

metallic copper at the AFM tip-integrated electrode, while the AFM tip was engaged to the sample surface in contact mode. In a consecutive step after imaging the sample surface, the probe was retracted from the surface by about 80 µm and the deposited copper was re-oxidized from the AFM-SECM tip using linear voltammetry allowing a semi-quantitative evaluation of the current peak area. The sensitivity of the amplifier of the SECM module limited the current range to ±100 nA, which resulted in saturation of the current for imaging experiments presented here. No post data software leveling correction was applied to any of the presented AFM images in order to evaluate the actual differences in height. Roughness values were calculated in base of the ISO 25178 norm, and values of the root mean square (rms) height of this evaluation provided.

2.3 Calibration

Prior to the dissolution experiments, calibration curves at the AFM-SECM probes were recorded in $CuSO_4$ solutions (stock solution 1 mM) to determine the limit of detection (LOD). Measurements were conducted in 5 mL of 0.5 M NaCl (pH = 3) adding incremental 25 / 50 µL steps of stock solution reflecting steps of 5 / 10 µM $CuSO_4$, respectively. A three-electrode set-up controlled by a potentiostat (CH-660A CH-Instruments, Austin, TX, USA) with an Ag/AgCl (sat.) and a platinum electrode as reference and counter-electrodes, respectively, was used. Copper deposition at the AFM tip-integrated gold frame electrode was obtained by first cathodically polarizing the tip at -0.4 V vs Ag/AgCl (sat.) during variable time periods. Then, the deposited copper was re-dissolved either using linear sweep voltammetry (LSV) with a scan rate of 50 mV s^{-1}, or square wave voltammetry (SWV). Parameters for SWV were as follows: 5 mV increments, 50 mV amplitude and 10 Hz frequency. The peak area in the potential range of -0.2 to 0 V was used for calibration purposes of the copper (II) content in solution.

3. Results and discussion

3.1 Calibration in standard solution

The response behavior of the AFM tip-integrated electrodes towards the quantitative determination of the copper content in solution was first explored. After a pre-deposition step at -0.40 V [40,43], copper was anodically stripped from the electrode using LSV or SWV while optimizing the pre-deposition step to a minimum time. The time, which is required for performing an AFM-SECM scan is typically 4-5 minutes. Therefore, deposition times were investigated in the range of 4 to 256 seconds. For these deposition times, the minimum copper concentration range revealing a linear correlation was in the micromolar range.

Some concerns arose from the signal response observed at the AFM tip-integrated electrodes during calibration. During the stripping step, the appearance of an anodic current peak at around +0.2 to +0.4 V following UPD at -0.4 V was expected for copper re-oxidation according to literature [40,43,44]. However, well-defined anodic peaks were obtained between -0.2 and 0 V, which correlated with the increasing copper (II) concentration at longer deposition times. Indeed, the observation of such stripping anodic current peaks in both potential windows, at -0.2 to 0 V and +0.2 to +0.4 V, during the copper stripping step has been reported elsewhere [45]. It was reported in literature that the peak at -0.2 to 0 V is predominantly associated with re-dissolution of the copper bulk deposit (Cu-Cu interaction), which is related to the lower required energy for dissolution in comparison to the peak at +0.2 to +0.4 V, which is associated to the re-dissolution of thin copper layers at gold surfaces (Cu-Au interaction) [45,46]. As a consequence, copper bulk

deposits require less anodic over-potential to be stripped into bulk solution, thus corresponding to the peak observed at around -0.2 to 0 V. Taking into account the small electrochemically active area of the AFM-SECM probes, this hypothesis is in excellent agreement with our observations, since the oxidizable Cu deposit directly attached to the small gold frame electrode (only re-dissolved at higher potentials, i.e., over +0.3 V) may scarcely produce any measurable signal considering the dimensions of the gold frame electrode (electrode area 0.26 μm^2). Hence, only the signal arising from the stripping of the copper bulk deposit actually resulted in a relevant and quantifiable response in the acidified chloride-containing solution.

Based on the integrated signals of the current peak obtained below 0 V, clear trends in respect to both copper concentrations and deposition times are observed. Figures 1A and 1B show the results with increasing copper concentration for a fixed pre-deposition time of 64 s, using LSV (Figure 1A) and SWV (Figure 1B), respectively. Also the effects of pre-deposition times were investigated (Figures 1C and 1D) at a fixed concentration of 29.7 µM copper sulphate. As displayed in Figure 1, increased current signals were obtained during the anodic re-dissolution with either higher copper cations concentration and/or longer copper pre-deposition times. As expected, current signals obtained with SWV resulted in enhanced detection compared to LSV. Hence, SWV was selected for quantification of the bulk copper concentration and for determining the analytical figures of merit. Figure 2A shows some representative square wave voltammograms from a calibration series obtained in a concentration range of 5 – 72 µM (added in 15 standard additions), while in Figure 2B, a calibration plot is presented (based on peak area evaluation). A linear correlation and comparatively small error bars for 3 repetitive measurements were obtained. Given the signal-to-noise ratio (SNR), the estimated limit of detection (LOD) and quantification (LOQ) were 14.8 and 19.6 µM, respectively. As the AFM-SECM module of the AFM system only offers the possibility to perform CV and LSV, only LSV could be used for semi-quantitative determination during imaging experiments.

3.2 Characterization of copper deposited on gold

3.2.1 Circular gold sample modified with copper

The disc-shaped gold sample and the AFM-SECM tip, immersed in 10 mM $CuSO_4$ / 50 mM H_2SO_4, solution were initially biased at +0.55 V to prevent any copper electro-reduction and deposition at either of the electrodes. Then, an interface region comprising a segment of the gold disc and the surrounding glass surface was imaged, as shown in the contact mode AFM topography image given in Figure 3A. The boundary between gold and glass is clearly visible (20 µm at the *x*-axis). The surface roughness of the gold surface is 17.8 ± 0.8 nm as expected for evaporated gold on glass. After imaging the glass / gold boundary, the tip was withdrawn and the gold sample was linearly polarized down to -0.25 V with a constant scan rate of 10 mV s^{-1}. After the applied potential reached -0.25 V, this potential was maintained for another 13 minutes resulting in clearly visible (optical microscope) copper crystal growth at the gold surface. The potential of the disengaged AFM-SECM probe was kept at +0.55 V during the copper deposition step, thus avoiding any undesired deposition of copper at the AFM-SECM tip. Then, the solution was exchanged to 0.5 M NaCl (pH = 3) using the flow-cell system. The sample was immediately biased at -0.30 V preventing any dissolution of the copper deposit. Then the sample was imaged again in contact mode with the AFM-SECM probe still polarized at +0.55 V. The topography of the copper deposit is shown in Figure 3B. The growth of stable copper crystals is clearly visible in the AFM images (topography and deflection shown in Figure 3B and 3C, respectively) and is also reflected by the increase in roughness (rms 90.5 ± 11.9 nm).

The AFM-SECM tip potential was then shifted to -0.40 V, and the potential of the sample was anodically swept at a constant rate of 1 mV s^{-1} while the AFM-SECM probe was constantly scanning the sample surface. Once a sufficiently anodic substrate potential of -0.15 V was reached, copper crystals started to dissolve. During this process, the topography and current recorded at the AFM tip-integrated electrode were simultaneously acquired, which are shown in Figure 4. AFM deflection images are presented as they reflect a better resolution of the process. A series of consecutive scans were continuously recorded with toggling scan direction from top to bottom and bottom to top as described in the figure caption. The scan velocity of the AFM-SECM probe was reduced to 8 µm s^{-1} for the combined measurements to minimize any convective effects due to the tip displacing some electrolyte volume while scanning. The first and third scans in Figures 4A and 4C were performed in scan direction from top to bottom, as depicted in the image; the second scan shown in Figure 4B started from the bottom. The dynamic evolution of the sample potential is marked with the dotted lines shown in the deflection and current images reflecting the actual substrate potential of the corresponding line scan. The linear sweep current response of the gold substrate during the re-oxidation of copper crystals deposited at the surface is shown in Figure 5A.

Changes in morphology, as shown in Figure 4 (deflection image, left) clearly indicate that the dissolution of the copper crystals becomes evident at a substrate anodic over-potential of -0.15 V. This dissolution process proceeds while the potential is swept for an additional 0.10 V, until ca. -0.05 V was reached, and consequently the surface morphology becomes similar to the initial gold surface, as copper crystals are no longer observable. This is also reflected by a major decrease of the substrate roughness. Roughness values were determined as average values of the roughness collected from five 1 x 1 μm^2 representative areas within the indicated dotted lines in Figure 4, i.e., while the substrate potential was close to the values indicated in the figure. Evaluating Figure 4, the sections of the scans taken at approximately the same locations on the surface for substrate potential values of -0.30 V and +0.15 V (Figures 4A and 4B, respectively) resulted in a decrease of the average roughness from 68.5 ± 26.4 nm to 16.4 ± 3.2 nm. Besides, the amperometric response of the gold sample in Figure 5A gives an anodic peak exactly in the potential region between -0.15 and 0 V, which clearly corresponds to copper re-oxidation as result of the anodic polarization visible in the deflection images depicted in Figure 4 (left). The baseline in the potential region of -0.3 to -0.18 V (Figure 5A) shows cathodic current values, which may be associated to the onset of the reduction of dissolved oxygen at the macroscopic gold substrate.

The subsequently released copper (II) cations were electrochemically collected at the AFM tip-integrated electrode biased at -0.40 V. The deposition of copper is clearly observable from the cathodic current appearing in the simultaneously recorded current images (Figure 4, right). A saturation of the cathodic currents (i.e., $\geq$ -100 nA) was observed. This current overload condition was actually expected, because a significant amount of copper ions is stripped from the macroscopic substrate and the AFM tip-integrated electrode is placed at a distance of about 400 nm (determined by the length of the AFM tip) above the sample surface. At this stage, we focused on a qualitative detection of the copper (II) ions as a function of the applied potential without quantification. The re-oxidation of copper deposited at the AFM-SECM probe after recording the images, as depicted in Figure 5B, resulted in a significant larger peak current compared to the currents recorded during calibration experiments.

A more detailed inspection of the image displayed in Figure 4A (right) revealed that copper (II) ions were locally detected even for cathodic potential values below -0.15 V. However, at that potential range, no significant anodic current evolution was observed at the sample (cf. Figure

5A), possibly due to the oxygen reduction current, which may overlay any anodic signal. Nevertheless, these first signs of copper collection at the tip, when moderate anodic over-potentials are applied may be assigned to distinct dissolving crystals, which are evident and marked with a circle in the deflection and tip current maps given in Figure 4A. Above -0.15 V, copper dissolution was observed mainly over the Cu-Au surface, and the edge could be easily distinguished (see position x = 22-23 µm in the scans of Figure 4, right). Furthermore, Figure 4B and 4C (right) reveal that copper ions are also detected at the AFM tip-integrated electrode over the region at x = 25 to 30 µm (i.e., the glass region adjacent to the embedded gold surface). This observation may be related to the geometry of the AFM-SECM probe and its eventually induced convective effects while moving; and/or alternatively from the fact that copper crystals may be dislocated and also be deposited at the glass surface surrounding the gold surface. The former may involve that given the distance from the tip-integrated electrode to the re-shaped AFM tip, the electrode may detect diffusing Cu^{2+} species few microns away from the glass / gold boundary, and also it might displace Cu(II)-rich electrolyte while moving across the boundary. However, homogeneously distributed currents would be expected from such convective effects, so the presence of copper crystals surrounding the gold surface may better satisfy the observations. Besides, when copper is subsequently re-dissolved, the crystals directly deposited at the boundary may be preferentially dissolved first. This may also explain the fact that no copper is detected within an approx. 3 µm region located between the interface and the area in x = 25 to 30 µm visible in Figures 4B and 4C.

3.2.2 Gold sample modified with individual copper crystals

In a second series of experiments, copper was deposited on a gold-coated silicon wafer by mild cathodic polarization of the substrate down to +0.10 V with a scan rate of 10 mV s^{-1} in 10 mM $CuSO_4$ / 50 mM H_2SO_4 solution. The sample was not further polarized at this potential and the electrolyte was immediately exchanged with 0.5 M NaCl (pH = 3) solution. The topography was imaged with substrate and tip biased at -0.30 and +0.55 V, respectively, preventing any metal release from the surface and/or its deposition at the AFM-SECM probe. Individual copper crystals were now observed as shown in Figure 6A. In a subsequent step, copper re-oxidation and imaging was performed as described above for the circular gold substrate. In order to better observe the dissolution sequence, topography images were rotated by 90 degrees. The substrate potential was anodically swept from -0.30 to +0.55 V at a scan rate of 1 mV s^{-1}, and the corresponding substrate current was monitored. Figure 6B reveals the topographical changes at the surface resulting from the dissolution of individual crystals at more positive potentials, while Figure 6C presents the current response obtained in three distinctive regions marked in Figure 6B with green dotted lines corresponding to regions of the substrate with different applied potentials (please also note the different current scales of the current maps presented in Figure 6C). The three potential regions correspond to distinct potential ranges applied to the substrate (see Figure 6D): the potential range between -0.25 to -0.15 V prior to the onset of anodic currents; the potential range between -0.15 and -0.025 V, the potential region of the anodic current peak is attributed to the re-oxidation of the bulk copper deposit; and a potential range from -0.025 to +0.20 V.

The AFM image of the sample does not reveal any significant topographic changes within the first 3 micrometers scanned in y direction (as marked by the second green dotted line) (Figure 6B), where the potential applied to the substrate was more cathodic than -0.15 V (Figure 6D). The current response recorded at the AFM-SECM probe was in the pA range, and mainly the stabilization and progressive depletion of a negative capacitive tip current, once tip potential was applied, was initially observed. When the potential of the substrate was close to -0.15 V (position

around y = 3 µm), the cathodic current recorded at the AFM-SECM started to increase, possibly as a result of the onset of copper dissolution from the sample and its subsequent collection at the tip.

As the scan proceeded and the potential was swept to -0.15 V, the measured cathodic current reached -100 nA (i.e., the saturation limit of the instrument) in the SECM response, which corresponds well with the potential window reflecting the substrate peak current as displayed in Figure 6D. Furthermore, copper crystals were progressively disappearing, which is evident in the corresponding region in Figure 6B. The detection of AFM-SECM tip current was mainly expected to occur above the single copper crystals present at the surface due to their preferential dissolution. Conversely, cathodic currents were predominantly measured also in areas without observable copper crystals. Moreover, much smaller current values were recorded when the AFM-SECM tip was scanning over the crystals (see green circle in Figure 6B and in the corresponding region of Figure 6C). This behavior may result from the dissolution of a homogeneous copper layer deposited at the surface prior (or simultaneous) to further growth of the crystals. In such case, copper would be homogeneously released from the substrate, and therefore detected across the entire exposed area at that given potential of the substrate. In fact, the dissolution may be more active from this surface than from the crystals depending on the inter-atomic interaction of the deposited metal and the corresponding energy levels, as anticipated above. With progressing scanned area and increased substrate potential of the AFM-SECM scan, the cathodic current detected at the AFM-SECM probe decreased by one order of magnitude again, as seen at the right image of Figure 6C. No copper crystals were further detected in the topography (Figure 6B) and no significant substrate current was observed (Figure 6D), although the tip records some cathodic current due to the reduction of copper (II) ions, presumably released in the previous step and still present in the diffusion layer.

The suggested homogeneous copper deposit was confirmed by EC-AFM experiments. If the gold electrode is less cathodically polarized during the copper deposition (i.e., the substrate potential was +0.2 V in $CuSO_4$ solution, and it was further maintained at this potential for 13 minutes), neither copper crystals nor relevant changes in roughness (from 1.99 to 2.24 nm before and after the deposition of copper, respectively) were observed. Also no changes in reflectivity of the sample (as observed with the optical microscope) could be detected. Yet, electrochemical signals arising from the re-oxidation of not only the copper monolayer directly attached to the gold electrode (at +0.336 V), but from a bulk copper deposit (at +0.022 V) were clearly detected [45,46]. Thus, copper is deposited at the substrate at the applied potential and conditions, which obviously involved the formation of few monolayers of copper with the first ones directly attached to the gold. Indeed, monitoring of copper layers on gold is reported to produce highly smooth surfaces, which can be followed by AFM if appropriate experimental conditions are chosen [47,48]. An estimation of the amount of copper (II), which was released during the first re-oxidation peak when only few copper layers are formed, gave a concentration around 10.6 µM in a volume confined below the AFM-SECM probe. Such concentration levels are, in principle, measurable with the AFM-SECM probes (see calibration experiments). However, if crystal formation is desired, more cathodic conditions like those used in experiments presented in Figures 4 and 6 must be applied. As a consequence, the amount of homogeneous copper deposit, which is first formed at the gold surface, may by far exceed the amount of crystals deposited at +0.2 V, and the subsequent copper re-oxidation from the gold substrate results in higher concentrations as expected from the visible amount of copper. Indeed, the integration of the current peak displayed in Figure 6D gives a total charge transfer 10^4 times bigger than the copper deposition performed at +0.2 V, and corresponds to a concentration in the 10 mM range. Hence, the current

saturation observed in Figure 6C due to the release of copper and the concentration of copper (II) close to the substrate appears reasonable.

In summary, if the copper deposition on gold is performed at conditions that only homogeneous copper layers are produced, the concentration level of released copper may remain within a quantifiable current range, although no topographical changes could be clearly identified. If the experimental parameters result in copper crystal growth, which can be clearly observed by AFM, the simultaneously monitored current response at the AFM-SECM probe will mostly reflect the release of the first homogeneous layers of copper, which exceeded the sensitivity of the used equipment.

3.3 Characterization of a pure copper sample

In a next step, a copper sheet as used in numerous real-word applications was investigated by AFM-SECM using a similar procedure as previously described for copper crystal-modified gold samples. However, in case of the copper sheet a constant substrate potential was applied during AFM-SECM imaging. A 25 x 25 μm^2 area of the surface was scanned at various substrate potential values while collecting copper (II) cations at the AFM-SECM probe polarized at -0.45 V. Copper re-oxidation from the AFM tip-integrated electrode was performed by LSV after each recorded image after the tip was retracted (80 µm from the surface). The sequence of substrate polarization values for the copper did not always follow an increasing progression. Instead, the surface was first cathodically protected at -0.45 V, and then sequentially polarized at -0.25, -0.19 and -0.13 V, respectively while scanning the same 25 x 25 μm^2 area. Then, the potential was shifted to more cathodic values (-0.15 and -0.17 V), in order to explore the effect of the activation-deactivation of the corroding material. Again the same area was imaged for each substrate potential. Finally, another five scans were successively recorded with the substrate polarized at -0.17 V to investigate if copper metal continues corroding while immersed into aggressive media despite anodic over-potentials being ceased or decreased. Representative AFM-SECM images are shown in Figure 7.

Figure 7 entails raw data, i.e., no post data treatment such as tilt correction or flattening was performed. The images displayed in Figure 7A were recorded at a substrate potential of -0.25 V, images in Figure 7B at a more positive potential of -0.19 V and in Figure C at -0.13 V. Figure 7D reflects the second scan of the consecutive series performed with the sample polarized at -0.17 V. Interesting topographic features, which changed with the applied potentials were observed in the regions marked as 1 and 2, highlighted in the maps with dotted circles. The dimensions of the marked features are given in Table 1. It cannot be excluded that the presented widths may be affected by possible imaging artefacts (double tip). From visual inspection of the representative scans, an inclusion, probably consisting in copper oxide or hydroxide is observed in the topography images depicted in Figure 7A for region 1, and in Figure 7B for both regions 1 and 2, respectively, which evolution differs. The height of the precipitate in region 1 remains constant in a range of 160-206 nm within almost all of the performed experiments, although its width increases up to 3 µm with increasing anodic over-potential from 1.78 µm in scan number 2 at -0.25 V (corresponding to Figure 7A) to 5.05 µm in scan number 4 at -0.13 V (corresponding to Figure 7C). Figure 7D reflects the scan with the sample biased at a more cathodic potential of -0.17 V (scan number 8, Table 1). At this potential, the precipitate appears to be smaller (decrease in width of approx. 600 nm), although it is still clearly visible in the following scans (measurements 5 to 10).

Conversely, the inclusion in region 2 does not appear until corrosion effectively occurs at the metal surface (see Figure 7B recorded at -0.19 V, showing an increase in current due to the detection of dissolved copper), which corresponds to scan number 3 in Table 1. In Figure 7C, (scan number 4), the activation of the sample at -0.13 V results in the inclusion becoming less evident in the AFM topography, although a carefully evaluation of the scan reflects the apparent growth of the precipitate up to maximum height and width values of 175 nm and 2.6 µm, respectively (cf. Table 1). A fact that may be related to the general passivation of the sample at these conditions, as discussed below. Next, a significant decrease in height was observed in scan 5 at a more negative potential of -0.15 V accompanied by a noticeable decrease in width to approx. 1.3 µm, indicating partial dissolution of the precipitate. Finally the change in height (as measured in the center of the spot) changes from a positive to a negative value in respect to the average height of the surrounding surface, which may be an indication that the inclusion dissolves and a pit is subsequently formed at the same spot, slowly propagating in the following measurements. The pit geometry can be seen in Figure 7D (scan number 8, Table 1), and is in good agreement with data obtained for corroding pits on copper with EC-AFM [36]. The simultaneously recorded current images (right side of Figure 7) show a distinctive current signal at the location of the precipitates, that is close to zero indicating that salt inclusions (region 1 in Figure 7A and region 2 in Figure 7B) confer local protection to the underlying metal surface, thereby preventing the dissolution of copper.

Also maximum height differences are observed within each scan with a maximum value of around 2 µm at a sample bias of -0.13 V (Figure 7C). However, such large topographic change suggests the existence of an apparent tilt in *y*-axis, with the lowest height values (arbitrarily shifted to z = 0 µm) observed at the maximum y coordinates (y = 25 µm). In contrast to images presented in Figure 4, measurements displayed in Figure 7 were always recorded from bottom to top. The measured height change (see Figure 7C) clearly increases during the scan acquisition, probably reflecting better the influence of the elapse of time during the constant polarization of the substrate, rather than a spatially localized phenomenon. It appears that the copper surface evolved with time by an increased passive layer at this potential, as a result of a solid-state reaction. This particular observation corresponds to the growth of the formed patina, more prominent at -0.13 V (see Figure 7C). Such homogeneous passivation phenomena of copper have been observed with EC-AFM [36]. This hypothesis is further supported by the roughness values obtained from 5 x 5 μm^2 sections of the scanned area, which are presented in Table 2. The area of the distinct precipitates (marked areas) has been avoided for determining the surface roughness. Roughness increase was expected to occur during the initial stages as the passive layer grows. This is mainly reflected from the increase of roughness values from 57.9 ± 0.2 nm to 137.6 ± 1.9 nm (N = 3) during the first 15 µm of the scan. In the second half of the scan, the surface roughness values decrease again, indicating that the surface progressively becomes smoother, possibly due to the oxide layer covering the interstitial spaces of the passive crystalline layer [49].

In general, the simultaneously recorded current image provides a distribution of active spots where cathodic current saturation occurs due to increased dissolution of copper. Such cathodic currents reflect the copper (II) generation at a large extent, and their subsequent collection at the AFM-SECM probe. The dissolution is negligible at the more cathodic potential value of -0.25 V (Figure 7A), which is clearly indicated by the AFM-SECM probe current in the pA range. When sufficient anodic over-potential is applied to the copper sample (i.e., -0.19 V, Figure 7B), spots of cathodic current are visible as a consequence of copper (II) evolution. These increased currents were expected to be more prominent at higher anodic substrate potential values of -0.13 and -0.17

V related to the more aggressive imposed conditions, which was observed as displayed in Figures 7C, and 7D, respectively. The fact that the recorded saturation in current was apparently more prominently detected in Figure 7D than in 7C, although a 40 mV lower over-potential was applied, can be explained considering that the higher anodic polarization of the copper substrate at the previous scan may lead to surface activation. This may induce continuing corrosion even after slightly reducing the applied corrosion potential, as the passive layer may continue degrading with time, so copper can still be released from even more spots.

The AFM-SECM probe current (integrated over time) acquired over the whole scanned area from each measurement is also given in Table 1. Increasing sample polarization up to -0.13 V (scan 4), results in a progressive damage of the passive layer, reflected by the further cathodic charge increase transferred from 0 to 2.93 µC. Even after reducing the anodic over-potential in scans 5 and 6 (potentials applied -0.15 and -0.17 V, respectively), a still increased transferred charge due to the collection of copper cations at the AFM-SECM probe is observed. The transferred charge value remained then within a range between 4.16 to 5.31 µC during the sequence 7 to 10 (-0.17 V), when passivation may occur at the end of the experimental series. The maximum transferred charge of 5.51 µC was observed in scan 6 (substrate bias of -0.17 V). This would equal to an estimated electro-reduction of 1.81 ng of copper (II).

Copper electrodeposited on the gold frame of the AFM tip-integrated electrode was re-dissolved by polarizing the AFM-SECM tip several times at 80 µm height after each recorded AFM-SECM image. Cyclic voltammetry was selected here for the re-dissolution of copper to ensure that copper had been completely stripped from the tip before performing the following AFM-SECM scan of the sequence, in case that more than one anodic sweep was needed to complete re-dissolution. Besides, the current detected at the AFM-SECM probe during the cathodic sweep of the voltammograms could be used for the evaluation of the still releasing copper cations from the surface. These experiments gave clear oxidation peaks for the first anodic sweep of the voltammogram, as depicted in representative measurements in Figure 8A. Table 1 also provides the calculated peak area of the forward (anodic) scan, as well as the limiting cathodic current values obtained at the most negative tip potential applied during the cathodic scan of the re-oxidation cycles. Such cathodic currents are attributed to the fact that these negative tip potentials enables the reduction of copper (II), which is generated at the substrate and diffuse from the substrate into bulk solution, since the copper substrate remained polarized at the potential values indicated at the *x*-axis of the graph. With the AFM-SECM probe positioned at a distance of 80 µm from the sample surface, copper (II) ions are still reduced at negative tip potentials in these SG-TC mode experiments.

As expected, no signal was observed for copper re-oxidation at the AFM-SECM probe after the first image was recorded with the substrate cathodically protected at -0.45 V. However, despite the absence of cathodic currents in the measurement performed at -0.25 V (Figure 7A, right), a small current peak of 1.22 nA in peak height giving an integrated area of 47.5 pA V (Figure 8A, red curve) was observed in the re-oxidation cycle recorded at the AFM-SECM probe. Such peak currents are similar to those obtained during the calibration experiments presented in Figure 1. The green LSV curve in Figure 1C, obtained in 29.7 µM $CuSO_4$ solution (deposition time of 256 s), gave a peak with an area of 21.7 pA V, comparable to the result from the peak observed in Figure 8 at -0.25 V substrate potential. As a first estimation, the peak presented in Figure 1C was obtained after a pre-deposition step, which reflects approximately the time that was required for recording half of the image (duration for recording the images presented in Figure 7 was approx. 420 seconds per image), and roughly amounts half of the transferred charge. Therefore, it is

assumed that the concentration of copper (II) ions within the gap between the AFM-SECM probe and the sample surface resulting from the homogeneous corrosion of copper in the passive regime conditions of the scan presented in Figure 7A, is around 29.7 µM, which corresponds well with the calibration data shown in Figure 1C. Moreover, no cathodic current could be clearly observed in respect to the background noise during the pre-deposition step of the measurements displayed in Figures 1 and 2. This correlates well with the absence of cathodic currents during the acquisition of the AFM-SECM scan, in spite of the subsequent appearance of an anodic peak during the copper re-oxidation from the tip in bulk solution. Hence, the technique is sensitive enough to determine quantitatively the metal produced during the apparently homogeneous copper corrosion, which occurs in such effective passive regime.

The subsequent application of higher substrate over-potentials (i.e., -0.13 and -0.15 V) results in current saturation during the following copper re-oxidation cycle from the AFM-SECM probe (cycle not shown), and a maximum in the peak area, as a result of a more vivid copper dissolution from the substrate surface. This is apparently contradictory to the data given in Figure 7C for the currents recorded during the AFM-SECM measurement with the substrate polarized at -0.13 V, which did not correspond to the measurement showing the highest cathodic currents. Again the current amplifier used during the experiments limits the sensitivity and detectable currents during imaging, and therefore prevents a quantitative evaluation of local features due to saturation. Hence, during the scan a significant amount of copper (II) may be generated at a few localized highly active spots (as can be derived from Figure 7B, right image) rather than homogeneously distributed partially active areas. Whereas in subsequent scans, the opposite trend may occur, translating in less amount of copper might be produced from larger areas. The copper re-oxidation from the AFM-SECM probe provides essential information on the actual extent of the anodic dissolution of the substrate. As expected, a maximum cathodic current was obtained during the re-dissolution cycle after performing AFM-SECM imaging at a substrate potential of -0.13 V, indicating maximum copper dissolution. The value -0.13 V was the most anodic potential of all conducted experiments. A progressive decrease in the anodic peak area and current during the cathodic sweep of the stripping cycles was observed for the following measurements at potentials of -0.15 and -0.17 V indicating the progressive decline of the attack, although still at corrosive conditions.

4. Conclusions

In this study, it was shown that AFM-SECM probes are ideally suitable for the analysis of surface corrosion processes. AFM-SECM can be used for the semi-quantitative determination of copper (II) ions released from copper samples, which were either electrochemically deposited copper crystals formed at gold substrates or pure copper specimen undergoing corrosion. Topographic changes originated from anodic degradation can be monitored while simultaneously recording spatially resolved electrochemical information related to the re-reduction of the released copper (II) ions at the AFM-SECM probe, thus providing correlated data on morphological changes and electroactivity. The dependence of the morphology and preferential dissolution of electrodeposited copper layers and crystals with parameters such as the applied substrate potential and the deposition time was explored. The spatial resolution during the detection and the re-oxidation of the copper collected at the AFM-SECM probe allows a semi-quantitative determination of the copper released from active spots, and the monitoring of anodic dissolution phenomena.

The electrochemical detection of local Cu^{2+} ions generated from a pure copper substrate during the initial stages of pit formation, as well as the local passivation of the surface due to the growth of corrosion products could be spatially resolved. The collection of minute amounts of copper (II) at the tip and the observed progressive changes in height evidenced the general passive regime and homogeneous passive layer formation. Again, AFM-SECM is suitable for the analysis of the mechanisms underlying apparently homogeneous corrosion processes at material surfaces and may thus provide novel insight into the corrosion-relevant behavior of passive layers including patina thickening and passive layer breakdown. Furthermore, localized phenomena occurring at the metal surface including precipitation and dissolution of protective corrosion products and pit nucleation and penetration may be accessible.

Acknowledgements

R. M.S., B.M.F.-P. and J.I. acknowledge the Spanish Ministry of Economy and Competitiveness (MINECO, Madrid) and the European Regional Development Fund, CTQ2012-36787. A Research Training Grant awarded to J.I. by the MINECO (*Programa de Formación de Personal Investigador*) is gratefully acknowledged. Short stay scholarships awarded to J.I. by the German Service of Academic Exchange (DAAD), and to J.I. and B.M.F.-P. by the University of La Laguna are thanked. The Focused Ion Beam Center UUlm, which is supported by FEI Company (Eindhoven, Netherlands), the German Science Foundation (INST40/385-F1UG), and the Struktur- und Innovationsfonds Baden-Württemberg are greatly acknowledged.

References

1. P. Marcus, F. Mansfeld (Eds.), Analytical Methods in Corrosion Science and Engineering. CRC Press, Boca Raton (FL, USA), 2006.
2. R. Oltra, V. Maurice, R. Akid, P. Marcus (Eds.), Local Probe Techniques for Corrosion Research. Woodhead Publishing, Cambridge (England), 2007.
3. D.E. Tallman, M.B. Jensen, Applications of scanning electrochemical microscopy in corrosion research. In: Scanning Electrochemical Microscopy, 2nd edition, A.J. Bard, M.V. Mirkin (Eds.), CRC Press, Boca Raton (FL, USA), 2012, pp. 451-468.
4. M.B. Jensen, D.E. Tallman, Application of SECM to Corrosion Studies. In: Electroanalytical Chemistry: A Series of Advances, Vol. 24, A.J. Bard, C. Zoski (Eds.). CRC Press, Boca Raton (FL, USA), 2012, pp. 171-286.
5. T. Missawa, H. Tanabe, In-situ observation of dynamic reacting species at pit precursors of nitrogen-bearing austenitic stainless steels, ISIJ International 36 (1996) 787-792.
6. K. Fushimi, M. Seo, An SECM observation of dissolution distribution of ferrous or ferric ion from a polycrystalline iron electrode, Electrochimica Acta 47 (2001) 121-127.
7. A.C. Bastos, A.M. Simões, S. González, Y. González-García, R.M. Souto, Imaging concentration profiles of redox-active species in open-circuit corrosion processes with the scanning electrochemical microscope, Electrochemistry Communications 6 (2004) 1212-1215.
8. R.M. Souto, Y. González-García, D. Battistel, S. Daniele, In situ scanning electrochemical microscopy (SECM) detection of metal dissolution during zinc corrosion by means of mercury sphere-cap microelectrode tips, Chemistry A European Journal 18 (2012) 230-236.

9. S.B. Basame, H.S. White, Scanning electrochemical microscopy of native titanium oxide films. Mapping the potential dependence of spatially-localized electrochemical reactions, Journal of Physical Chemistry 99 (1995) 16430-16435.
10. C.H. Paik, H.S. White, R.C. Alkire, Scanning electrochemical microscopy detection of dissolved sulfur species from inclusions in stainless steel, Journal of The Electrochemical Society 147 (2000) 4120-4124.
11. K. Mansikkamäki, P. Ahonen, G. Fabricius, L. Murtomäki, K. Kontturi, Inhibitive effect of benzotriazole on copper surfaces studied by SECM, Journal of The Electrochemical Society 152 (2005) B12-B16.
12. M.B. Jensen, A. Guerard, D.E. Tallman, G.P. Bierwagen, Studies of electron transfer at aluminum alloy surfaces by scanning electrochemical microscopy, Journal of The Electrochemical Society 155 (2008) C324-C332.
13. B.M. Fernández-Pérez, J. Izquierdo, S. González, R.M. Souto, Scanning electrochemical microscopy studies for the characterization of localized corrosion reactions at cut edges of coil coated steel, Journal of Solid State Electrochemistry 18 (2014) 2983-2992.
14. K.A. Ellis, M.D. Pritzker, T.Z. Fahidy, Modeling the degradation of scanning electrochemical microscope images due to surface roughness, Analytical Chemistry 67 (1995) 4500-4507.
15. Y. González-García, J.J. Santana, J. González-Guzmán, J. Izquierdo, S. González, R.M. Souto, Scanning electrochemical microscopy for the investigation of localized degradation processes in coated metals, Progress in Organic Coatings 69 (2010) 110-117.
16. L. Guadagnini, C. Chiavari, C. Martini, E. Bernardi, L. Morselli, D. Tonelli, The use of scanning electrochemical microscopy for the characterisation of patinas on copper alloys, Electrochimica Acta 56 (2011) 6598-6606.
17. Y. González-García, S.J. García, A.E. Hughes, J.M.C. Mol, A combined redox-competition and negative-feedback SECM study of self-healing anticorrosive coatings, Electrochemistry Communications 13 (2011) 1094-1097.
18. V. Maurice, P. Marcus, Scanning tunneling microscopy and atomic force microscopy. In: Analytical Methods in Corrosion Science and Engineering, F. Mansfeld, P. Marcus (Eds.). CRC Press, Boca Raton, (FL, USA), 2006, Ch. 5.
19. U.K. Mudali, N. Padhy, Electrochemical scanning probe microscope (EC-SPM) for the in situ corrosion study of materials: an overview with examples, Corrosion Reviews 29 (2011) 73-103.
20. M. Ludwig, C. Kranz, W. Schuhmann, H.E. Gaub, Topography feedback mechanism for the scanning electrochemical microscope based on hydrodynamic forces between tip and sample, Review of Scientific Instruments 66 (1995) 2857-2860.
21. A. Hengstenberg, C. Kranz, W. Schuhmann, Facilitated tip-positioning and applications of non-electrode tips in scanning electrochemical microscopy using a shear force based constant-distance mode, Chemistry A European Journal 6 (2000) 1547-1554.
22. M.A. Alpuche-Aviles, D.O. Wipf, Impedance feedback control for scanning electrochemical microscopy, Analytical Chemistry 73 (2001) 4873-4881.
23. A.S. Baranski, P.M. Diakowski, Application of AC impedance techniques to scanning electrochemical microscopy, Journal of Solid State Electrochemistry 8 (2004) 683-692.
24. K. Eckhard, W. Schuhmann, Alternating current techniques in scanning electrochemical microscopy (AC-SECM), Analyst 133 (2008) 1486-1497.
25. C. Kranz, Recent advancements in nanoelectrodes and nanopipettes used in combined scanning electrochemical microscopy techniques, Analyst 139 (2014) 336-352.

26. A. Davoodi, J. Pan, C. Leygraf, S. Norgren, In situ investigation of localized corrosion of aluminum alloys in chloride solution using integrated EC-AFM/SECM techniques, Electrochemical and Solid-State Letters 8 (2005) B21-B24.
27. A. Davoodi, J. Pan, C. Leygraf, S. Norgren, Integrated AFM and SECM for in situ studies of localized corrosion of Al alloys, Electrochimica Acta 52 (2007) 7697-7705.
28. A. Davoodi, J. Pan, C. Leygraf, S. Norgren, Multianalytical and in situ studies of localized corrosion of EN AW-3003 alloy – influence of intermetallic particles, Journal of The Electrochemical Society 55 (2008) C138-C146.
29. J. Izquierdo, A. Eifert, R.M. Souto, C. Kranz, Simultaneous pit generation and visualization of pit topography using combined atomic force–scanning electrochemical microscopy, Electrochemistry Communications 51 (2015) 15-18.
30. J. Izquierdo, A. Eifert, C. Kranz, R.M. Souto, In situ monitoring of pit nucleation and growth at an iron passive oxide layer by using combined atomic force and scanning electrochemical microscopy, ChemElectroChem 2 (2015) 1847-1856.
31. Y. Feng, K.S. Siow, W.K. Teo, K.L. Tan, A.K. Hsieh, Corrosion mechanisms and products of copper in aqueous solutions at various pH values, Corrosion 53 (1997) 389-398.
32. S. González, M. Pérez, M. Barrera, A.R. González-Elipe, R.M. Souto, Mechanism of copper passivation in aqueous sodium carbonate-bicarbonate solution derived from combined X-ray photoelectron spectroscopic and electrochemical data, Journal of Physical Chemistry B 102 (1998) 5483-5489.
33. J.L. Lei, L.J. Li, S.M. Cai, S.T. Zhang, D. Li, M.Z. Yang, Effect of Cl^- on the corrosion behaviour of copper electrode in weak-alkaline medium, Acta Physico-Chimica Sinica 17 (2001) 1107-1111.
34. J.Y. Josefowicz, L. Xie, G.C. Famington, Observation of intermediate CuCl species during the anodic dissolution of Cu using atomic force microscopy, Journal of Physical Chemistry 97 (1993) 11995-11998.
35. J. Li, D. Lampner, In-situ AFM study of pitting corrosion of Cu thin films, Colloids and Surfaces A 154 (1999) 227-237.
36. G. Bertrand, E. Rocca, C. Savall, C. Rapin, J.-C. Labrune, P. Steinmetz, In-situ electrochemical atomic force microscopy studies of aqueous corrosion and inhibition of copper, Journal of Electroanalytical Chemistry 489 (2000) 38-45.
37. J. Izquierdo, J.J. Santana, S. Gonzalez, R.M. Souto, Uses of scanning electrochemical microscopy for the characterization of thin inhibitor films on reactive metals: the protection of copper surfaces by benzotriazole, Electrochimica Acta 55 (2010) 8791-8800.
38. C. Li, L. Li, C. Wang, Study of the inhibitive effect of mixed self-assembled monolayers on copper with SECM, Electrochimica Acta 115 (2014) 531- 536.
39. E. Martinez-Lombardia, Y. Gonzalez-Garcia, L. Lapeire, I. De Graeve, K. Verbeken, L. Kestens, J.M.C. Mol, H. Terryn, Scanning electrochemical microscopy to study the effect of crystallographic orientation on the electrochemical activity of pure copper, Electrochimica Acta 116 (2014) 89-96.
40. D. Ruhlig, W. Schuhmann, Spatial imaging of Cu^{2+}-ion release by combining alternating current and underpotential stripping mode scanning electrochemical microscopy, Electroanalysis 19 (2007) 191-199.
41. A.S. Lima, M.O. Salles, T.L. Ferreira, T.R.L.C. Paixão, M. Bertotti, Scanning electrochemical microscopy investigation of nitrate reduction at activated copper cathodes in acidic medium, Electrochimica Acta 78 (2012) 446- 451.

42. C. Kranz, G. Friedbacher, B. Mizaikoff, A. Lugstein, J. Smoliner, E. Bertagnolli, Integrating an ultramicroelectrode in an AFM cantilever: combined technology for enhanced information, Analytical Chemistry 73 (2001) 2491-2500.
43. J. Zhuang, L. Zhang, W. Lu, D. Shen, R. Zhu, D. Pan, Determination of trace copper in water samples by anodic stripping voltammetry at gold microelectrode, International Journal of Electrochemical Science 6 (2011) 4690-4699.
44. A.P.R. de Souza, A.S. Lima, M.O. Salles, A.N. Nascimento, M. Bertotti, The use of a gold disc microelectrode for the determination of copper in human sweat, Talanta 83 (2010) 167-170.
45. J.F. Huang, B.-T. Lin, Application of a nanoporous gold electrode for the sensitive detection of copper via mercury-free anodic stripping voltammetry, Analyst 134 (2009) 2306-2313.
46. G. Herzog, D.W.M. Arrigan, Determination of trace metals by underpotential deposition–stripping voltammetry at solid electrodes, Trends in Analytical Chemistry 24 (2005) 208-217.
47. S. Manne, P.K. Hansma, J. Massie, V.B. Elings, A.A. Gewirth, Atomic-resolution electrochemistry with the atomic force microscope: copper deposition on gold, Science 251 (1991) 183-186.
48. N. Ikemiya, S. Miyaoka, S. Hara, In situ observations of the initial stage of electrodeposition of Cu on Au(100) from an aqueous sulfuric acid solution using atomic force microscopy, Surface Science 327 (1995) 261-273.
49. B.R. Lewandowski, D.A. Lytle, J.C. Garno, Nanoscale investigation of the impact of pH and orthophosphate on the corrosion of copper surfaces in water, Langmuir 26 (2010) 14671-14679.

Table 1. Data analysis of the AFM-SECM scans obtained at the solid copper sample. The evolution of the charge transferred during the SECM acquisition, and the height and width of features in regions 1 and 2 marked in Figure 7, the peak area obtained from the Anodic Stripping Voltammetry (ASV), and the current response are presented

Scan No.	Substrate potential / V	Region 1		Region 2		Charge transferred (SECM) / µC	ASV peak area / nA V	ASV SG-TC response / nA
		Height / nm	Width / µm	Height / nm	Width / µm			
1	-0.45	180	1.98	--	--	--	--	--
2	-0.25	195	1.78	--	--	$-1.12 \cdot 10^{-3}$	0.0475	0.0488
3	-0.19	167	3.42	158	2.26	-0.430	0.773	-0.131
4	-0.13	177	5.05	175	2.64	-2.93	19.1	-6.12
5	-0.15	160	4.40	61.8	1.33	-4.51	10.5	-2.32
6	-0.17	186	4.38	-115	1.45	-5.51	0.687	-0.278
7	-0.17	200	4.99	-118	1.46	-4.16	1.28	-0.385
8	-0.17	192	4.31	-153	2.44	-4.80	0.779	-0.320
9	-0.17	206	4.40	-176	2.15	-4.72	0.797	-0.317
10	-0.17	327	3.61	-175	2.44	-5.31	0.539	-0.259

Table 2. Roughness evolution measured at selected 5 x 5 µm^2 (N = 3) areas extracted from the image displayed in Figure 7C at the reported interval of the *y*-axis. Data presented in chronological order as they were obtained during the scan acquisition, starting from *y* = 25 µm to *y* = 0 µm.

***y* axis interval / µm**	**rms / nm**
20 to 25	57.9 ± 0.2
15 to 20	121.2 ± 1.2
10 to 15	137.6 ± 1.9
5 to 10	117.2 ± 2.1
0 to 5	85.8 ± 4.0

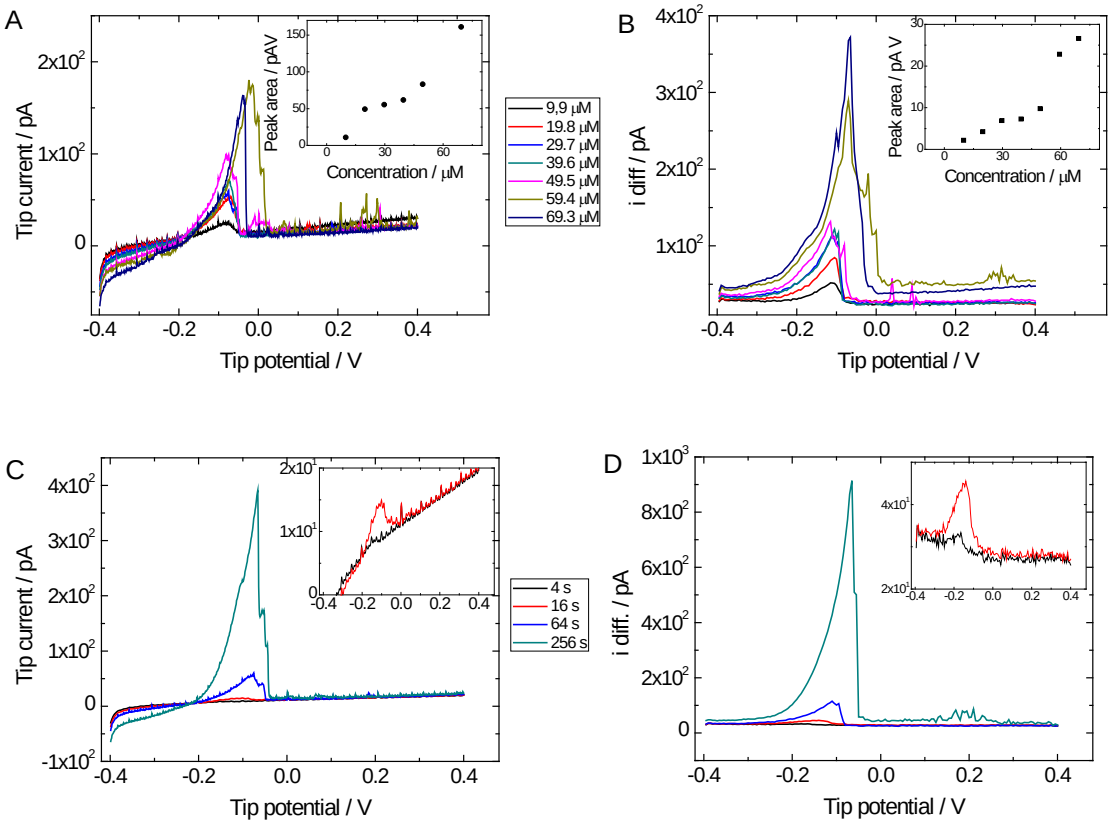

Figure 1. Voltammetry recorded at an AFM-SECM probe (A,B) in varying copper sulphate concentrations using a fixed deposition time of 64 s at -0.40 V prior to stripping, and (C,D) voltammograms recorded at varying deposition times at a fixed $CuSO_4$ concentration of 29.7 µM. Anodic stripping was obtained using LSV (A,C) or SWV (B,D). Insets in (A) and (B) give the peak area vs. Cu(II) concentration, whereas insets in (C) and (D) display the magnification of the signals acquired for 4 s and 16 s deposition time. Parameters for anodic stripping LSV and SWV are given in the experimental section. Electrolyte: 0.5 M NaCl (pH = 3).

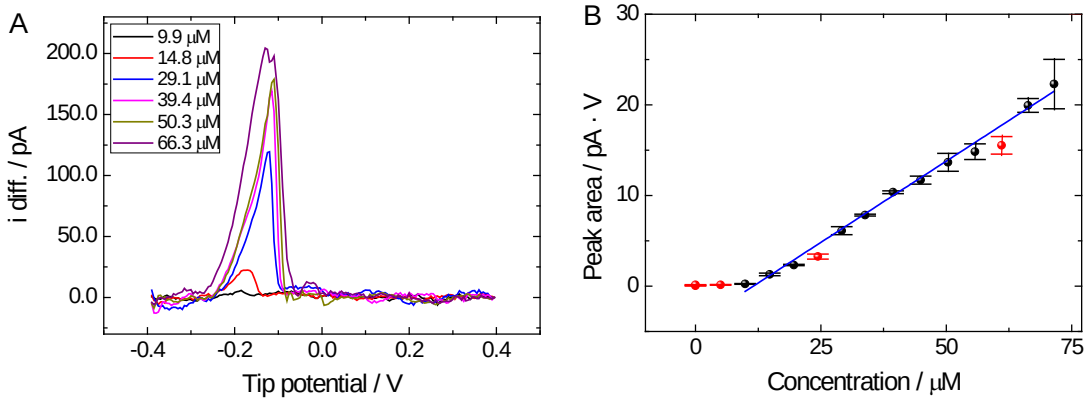

Figure 2. Calibration of the AFM tip-integrated electrode towards increasing $CuSO_4$ concentrations using SWV. Deposition time was fixed at 30 s. The error bars reflect 3 measurements. Electrolyte: 0.5 M NaCl (pH = 3).

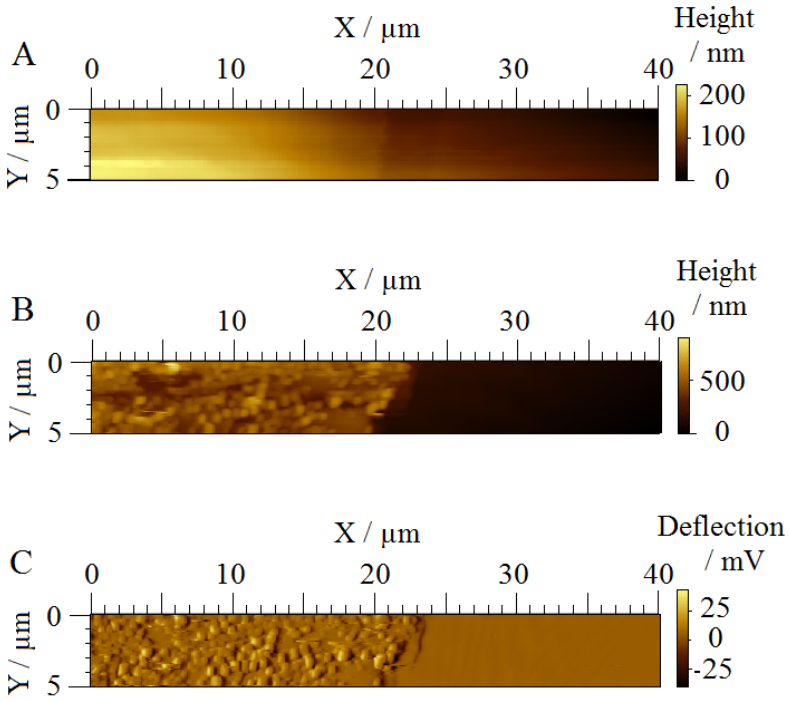

Figure 3. Contact mode AFM images recorded at the gold-glass boundary of the disc-shaped gold substrate: (A,B) topography and (C) deflection with image reflecting the surface (A) before and (B,C) after electrochemical copper deposition. The sample was immersed in (A) 10 mM $CuSO_4$ / 50 mM H_2SO_4 solution and (B,C) in 0.5 M NaCl (pH = 3) solution, while the sample was polarized at (A) +0.55 and (B,C) -0.30 V. During imaging the AFM-SECM probe potential was maintained at +0.55 V. Scan rate: 25 µm s^{-1}.

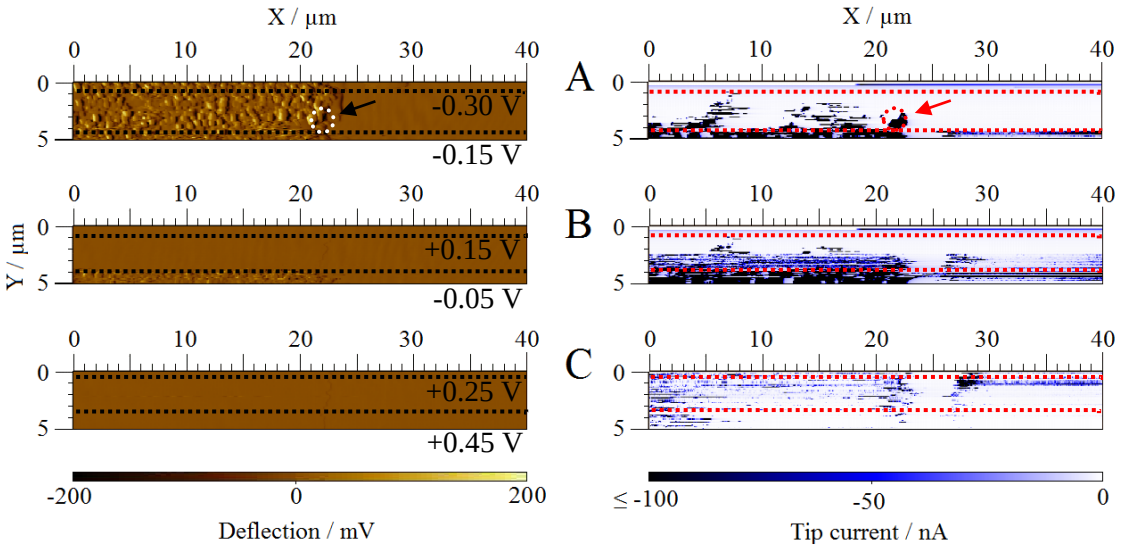

Figure 4. AFM-SECM images acquired in 0.5 M NaCl (pH = 3) during copper dissolution from the gold-glass sample: (left) contact mode AFM deflection images and (right) faradaic current plots recorded at the AFM-SECM probe (square-shaped gold frame electrode: 750 nm edge length, re-shaped AFM tip height: 400 nm). Tip potential was maintained at -0.40 V, while the sample potential was anodically scanned from -0.30 V to +0.50 V at a constant scan rate of 1 mV s^{-1}. Successive scans were recorded with toggling scan direction (A,C) from top to bottom and (B) from bottom to top. The potential values below the dotted lines in the deflection images indicate the potentials applied when tip was acquiring the given line. Scan rate: 8 µm s^{-1}.

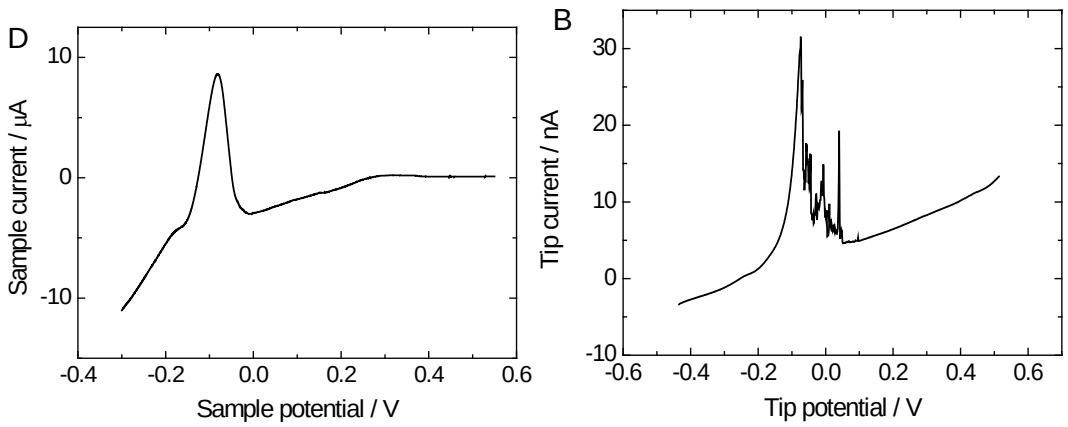

Figure 5. The scan in (A) depicts the copper re-oxidation produced at the gold substrate in 0.5 M NaCl (pH = 3) solution; scan rate: 1 mV s^{-1}. The scan in (B) was recorded at the AFM-SECM probe after the scan represented in Figure 4 was acquired and the AFM-SECM probe was retracted 80 µm from the sample surface; scan rate: 50 mV s^{-1}.

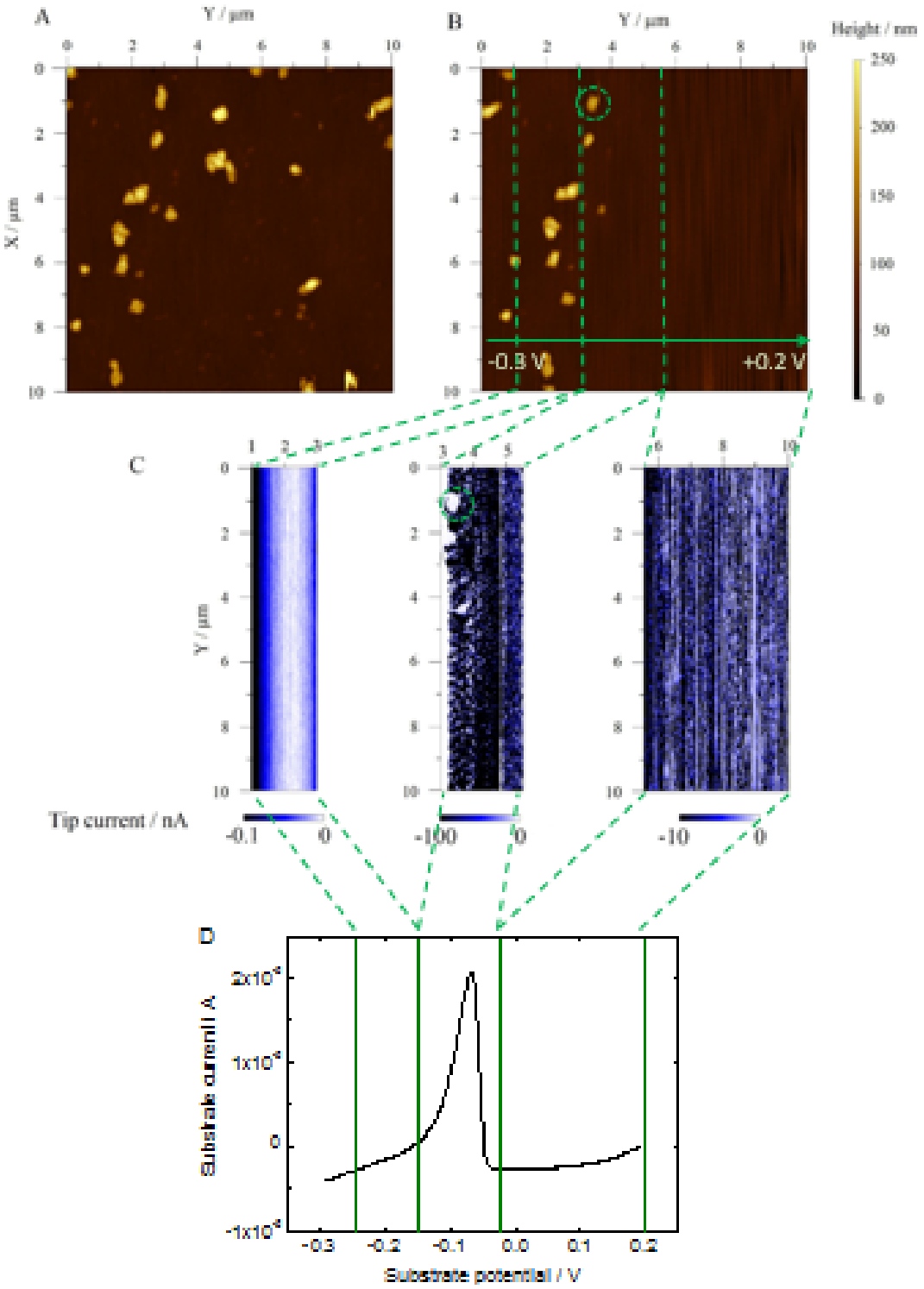

Figure 6. AFM-SECM data obtained in 0.5 M NaCl (pH = 3) during the re-oxidation of the copper crystals formed at a bare gold surface. Green-dotted lines correlate the scanned areas and the potential window applied to the substrate while acquiring the images. (A,B) AFM topography images recorded in contact mode of the surface (A) before and (B) during copper re-oxidation. (C) SECM response of the tip while scanning the corresponding areas marked in (B) (square-shaped gold frame electrode: 750 nm edge length, re-shaped AFM tip height: 400 nm). (D) Substrate current response versus the applied potential measured while the AFM-SECM probe was acquiring the data displayed in (B) and (C).

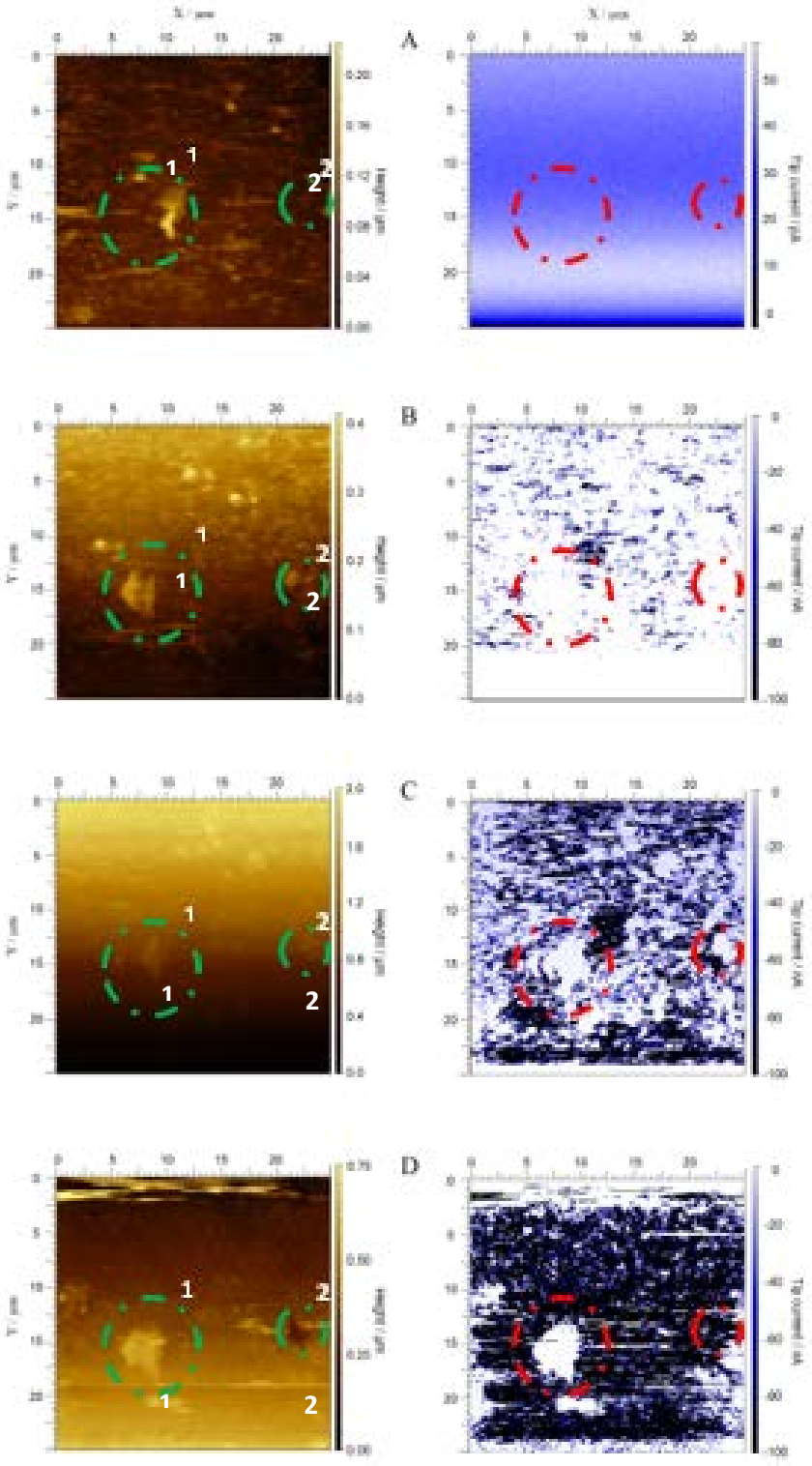

Figure 7. AFM-SECM images obtained of a polished solid copper sample immersed in 0.5 M NaCl (pH = 3); topography (left) and current image recorded with the AFM tip-integrated electrode (square-shaped gold frame electrode: 1.02 µm edge length, re-shaped AFM tip height: 420 nm) (right), while subsequently polarizing the substrate at (A) -0.25 V, (B) -0.19 V, (C) -0.13 V and (D) -0.17 V. The scan direction was bottom to top for the recorded image sequence. Scan dimensions: 25 x 25 μm^2; AFM tip-integrated electrode potential: -0.45 V; scan rate 30 $\mu m\ s^{-1}$. Images were acquired in the A-to-D sequence.

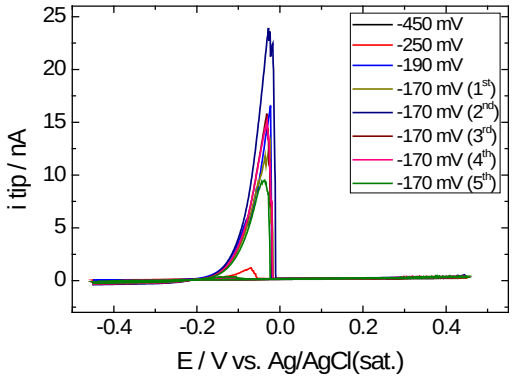

Figure 8. Cyclic voltammetry corresponding to the copper re-oxidation from the tip once withdrawn at 80 µm height into the bulk 0.5 M NaCl (pH = 3) solution after the AFM-SECM scan acquisition. Scan rate: 50 mV s^{-1}. Legend in *x*-axis indicates the substrate potential applied during the re-oxidation experiments and the previous AFM-SECM scans, chronologically ordered as they were acquired.